Materials Advances

ROYAL SOCIETY OF CHEMISTRY

PAPER

View Article Online
View Journal | View Issue

Cite this: *Mater. Adv.*, 2026, 7, 3004

Exploring sustainable water treatment: comprehensive analysis of an NZS-D nanocomposite for enhanced dye adsorption

Md. Sajid,[ab] Mohammed K. Al Mesfer,[cd] Mohd Danish,[cd] Atul Sharma[a] and Saif Ali Chaudhry *[a]

In this study, an innovative hybrid nanocomposite, abbreviated as NZS-D, was developed by incorporating nickel and zinc binary sulphide nanoparticles into the organic framework of date seed grains through a straightforward co-precipitation technique. The synthesized NZS-D was comprehensively characterized using various spectroscopic techniques which confirmed the presence of abundant functional groups on the NZS-D surface, porous morphology, and grain size range of 70–90 nm. The NZS-D was investigated for its capability to remediate polluted water through adsorption of two model dyes, one cationic, *i.e.*, Nile blue, and the other anionic, *i.e.*, Congo red, from simulated wastewater in the batch method. The process was investigated to check the influence of water pH, temperature, dye concentration, NZS-D dosage, and contact time, on the sorption capacity. Remarkably, the maximum sorption capacity (Q_{max}) reached to 208.333 and 121.951 mg g^{-1} for Congo red and Nile blue, respectively, under optimized conditions. The sorption was found to be thermodynamically feasible, physicochemical process governed by the weak Van der Waals forces or electrostatic interaction between the functional groups at the NZS-D surface and the dye molecules in water. The mechanisms of the preparation of NZS-D and the sorption process have been thoroughly investigated and explained.

Received 29th October 2025,
Accepted 21st January 2026

DOI: 10.1039/d5ma01245g

rsc.li/materials-advances

1. Introduction

Water resources are confronting with a grave peril arising from the flow of toxic anthropogenic contaminants. Commercial synthetic dyes are a major contributor to this predicament which exacerbates existing water scarcity crisis and pose substantial risk to the environment and human health.[1] The discharge of huge volume of dye-laden wastewater into natural water bodies is a major concern and high visibility made it one of the first contaminants to be identified and recognized.[2] The industrial wastewater poses a severe threat to the environment, and human health, therefore, it has led to debates and legislative actions. The remediation of wastewater, especially the removal of synthetic dyes and other pollutants, is garnering attention worldwide. Industrial sectors, such as the textile, paper, paint, plastic, pesticide, and pharmaceutical sectors are major contributor of wastewater containing synthetic dyes.[3,4] The synthetic dyes are well-known harmful pollutants that trigger allergic dermatitis, genetic mutations and ultimately cancer of human body.[5] The presence of dyes in wastewater has reached a critical level which necessitate efficient removal methods to reduce their harmful impact on human being. Among the synthetic dyes, high concentrations of Congo red (CR) in water is toxic to human and can be fatal and consumption has been reported to cause cancer and cytotoxicity, including genotoxicity, hemotoxicity, and neurotoxicity, in addition to respiratory and reproductive disorders.[6] Furthermore, CR has been linked to platelet aggregation, thrombocytopenia, and occurrence of disseminated micro-embolism which arises due to reductions in blood protein content.[7] Similarly, Nile blue (NB) can cause cancers, allergies, and renal complexities.[8] Consequently, the world urgently requires the development of economical methods for eliminating synthetic dyes from wastewater before its discharge into water sources. Numerous conventional methods are in use for treatment of wastewater to remove dyes, including biological treatment,[9] coagulation,[10] electrochemical,[11] adsorption,[12,13] oxidation,[14] catalytic reduction[15,16] and membrane filtration.[17] Among these, adsorption has emerged as a prominently favoured choice owing to its cost-effectiveness, straightforward design, operational simplicity, and generation of minimal toxic waste.

[a] *Department of Chemistry, Jamia Millia Islamia, New Delhi-110025, India. E-mail: schaudhry@jmi.ac.in*
[b] *Department of Chemistry, B.P Mandal College of Engineering, Madhepura-852128, India*
[c] *Central Labs, King Khalid University, AlQura'a, P.O. Box 960, Abha, Saudi Arabia*
[d] *College of Engineering, Department of Chemical Engineering, King Khalid University, AlQura'a, P.O. Box 960, Abha, Saudi Arabia*

Sulphides of transition metals, such as Ni, Zn, *etc.*, have gained considerable attention across various fields because of their distinct crystal structures and chemical behaviour. Transition metal sulphide nanoparticles have significant specific surface area which make them potential adsorbents for dyes or other pollutants removal from wastewater. For example, in one study, nickel sulphide was synthesized, through a ball-milling method, and employed for the adsorptive removal of Methylene blue.[18] Another study was focused on the efficient removal of Crystal violet and Biebrich scarlet dyes.[19] In 2019, Chowdhury *et al.*, 2019, developed Ni–Co–S/SDS, a proficient and economically viable nanocomposite for the elimination of water pollutants.[20] The sorption capacity of metal sulphides for the removal of dyes, from wastewater, has been enhanced by functionalizing them with carboxymethyl-cellulose, chitosan, and natural polymers. Additionally, agricultural and industrial wastes, in either unaltered or modified form, are alternative materials with reduced costs, for water remediation.

Date seeds, a waste product, contains polyphenolics, phenolic acid, carotenoids, fibre, fat, protein, minerals, and various other functional compounds. It has been considered as an inexpensive, effective adsorbing material; however, only limited research has been reported. Mahdi *et al.*, 2018, have investigated the use of date-seed-derived biochar for heavy metal remediation from wastewater.[21] In another study, date-seed biochar has exhibited 99% removal efficiency for Cu^{2+} and Ni^{2+}.[22] However, additional modification and detailed investigation of date seed powder, as an adsorbent, is required to produce materials with enhanced stability and adsorption efficiency. The present study was aimed to evaluate the potential of nanocomposite produced by embedding nickel–zinc binary sulphide nanoparticles into date seed grains which has improved stability and adsorption capacity of the date seed grains. The prepared NZS-D was investigated for the removal of two model dyes, CR and NB, from simulated wastewater, in a batch system. The NZS-D was characterized using infrared spectroscopy (FT-IR), powder X-ray diffraction (P-XRD), ultraviolet-visible (UV-Vis) spectroscopy, field emission scanning electron microscopy (FE-SEM), transmission electron microscopy (TEM), elemental analysis (EDX), zeta potential measurement and thermogravimetric analysis (TGA). The nanocomposite displayed a remarkable maximum adsorption capacity of 208.33 and 121.95 mg g^{-1} for CR and NB dyes, respectively. Its facile synthesis, high sorption capacity and cost-effectiveness make NZS-D a potential nanocomposite for water treatment.

2. Experimental section

2.1 Materials

$Ni(OAc)_2{\cdot}4H_2O$ and C_2H_5NS (thioacetamide) were obtained from Sisco Research Laboratories, while AR-grade $ZnSO_4{\cdot}7H_2O$ was sourced from S D Fine-chem. Ltd, New Delhi. CR and NB dyes were obtained from Loba Chemie Pvt. Ltd, New Delhi. Date seed powder was purchased from Distihub Pvt. Ltd, New Delhi. Laboratory-prepared double-distilled water was used throughout the experiment.

2.2 Preparation of NZS-D

The NZS-D was prepared, through a co-precipitation method, using $Ni(OAc)_2{\cdot}4H_2O$, $ZnSO_4{\cdot}7H_2O$, C_2H_5NS and date seed powder. Both nickel acetate and zinc sulphate salts were dissolved in 100 mL of distilled water so that each had a 0.1 M concentration. In another flask, 1.0 g date seed powder was dispersed in distilled water, and the dispersion was then poured into the metal ion mixture and sonicated. The saturated dispersion was stirred magnetically at 90 °C for 1 h. In another beaker, 0.3 M thioacetamide solution was prepared, sonicated, and then added dropwise to the dispersion prepared above. The resulting reaction mixture was stirred for another 2 h at 90 °C. The reaction mixture was neutralized to precipitate the binary metal sulphide, then cooled and centrifuged. The precipitate was washed with distilled water multiple times and then oven-dried at a mild temperature.[20]

2.3 Instrumentation and characterization

A detailed investigation was performed to ascertain the surface characteristics of the synthesised NZS-D using various analytical techniques. The IR spectrum was recorded using a Bruker Tensor 37 spectrometer, equipped with ATR mode in the range of 4000–600 cm^{-1}. HR-TEM images of NZS-D were captured using the TECHNAI G20 HR-TEM (Thermo Scientific Company), operated at 200 kV, to study the morphology of the synthesized binary sulphide nanoparticles. The optical properties of the NZS-D were investigated by recording the UV-vis spectrum with a T-80 UV-vis spectrophotometer.

The powder XRD crystallographic analysis was carried out, using a Rigaku X-ray diffractometer equipped with Cu Kα radiation (λ = 1.5419 Å), to obtain the diffraction pattern of the NZS-D. High resolution-SEM imaging was also conducted using a ZEISS microscope (EVO18) integrated with EDS to investigate the surface microstructure. The thermal stability of NZS-D was investigated by recording its TGA plot using a LABSYS EVOTGADSC 131 EVO analyzer (SETARAM Instrumentation, France) in the temperature range of 25–800 °C under N_2 atmosphere. The surface charge of NZS-D was determined, in terms of zeta potential, using a Malvern Zetasizer Nano-ZS analyzer. These characterizations played a crucial role in understanding the mechanism of the formation of the NZS-D nanocomposite and its interactions with dyes during adsorption.

2.4 Dye sorption experiment

The adsorption efficacy of the prepared NZS-D nanomaterial was explored for the adsorptive remediation of NB and CR dyes from wastewater through batch-mode experiment. The simulated contaminated water was prepared, from aqueous stock solutions, by dissolving fixed weights of NB and CR dyes in laboratory-prepared double-distilled water. Subsequent dilutions were carried out to achieve the required 10–60 mg L^{-1} concentrations. The sorption investigations were first carried out with 10 mL solutions of each dye in a set of 50 mL

Erlenmeyer flasks and a fixed weight of NZS-D in each flask to optimize the dosage, concentration, time, pH, *etc.* The Erlenmeyer flasks were mechanically stirred in a water bath shaker at 150 rpm and after certain time the supernatants were removed from each set, and the unadsorbed dye concentrations were determined spectrophotometrically.[23] The sorption performance of NZS-D, towards NB and CR, was evaluated by substituting the experimental sorption data into mathematical relationships (eqn (1) and (2)).[20,24] The obtained sorption parameters were utilized to gain valuable insights into the potential application of NZS-D for the commercial-scale development of wastewater treatment systems.

$$Q_e = (C_0 - C_e)V/m \quad (1)$$

$$\%\text{Removal} = \frac{(C_0 - C_e)}{C_0} \times 100 \quad (2)$$

The symbols C_0 and C_e represent the initial and equilibrium concentration of dyes, respectively, while V and m indicate volume of the solution used in each experiment and mass of NZS-D employed in the study.

2.5 Batch adsorption experiments

The contact time, dosage of NZS-D, concentrations of CR and NB, pH of dyes solutions, and temperature, were optimized in batch-mode sorption experiments. For dosage optimization, the sorption experiments were performed with different weights of NZS-D for CR and NB dyes solutions at normal temperature and neutral pH. For this, 10 mL of 20 mg L^{-1} NB or CR solution was taken in a conical flask and supplemented with 0.5 to 2.5 g L^{-1} dosage of NZS-D. These reaction mixtures were agitated for 2 h at room temperature in a mechanical water bath shaker. The result revealed that the removal of these dyes reached saturation at a 0.5 g L^{-1} dosage of NZS-D for CR, and 1.0 g L^{-1} for NB. Thereafter, no substantial variation in the extent of removal was observed, and consequently, these weights were selected as the optimized dosages for the entire study.

The impact of contact time on the percentage remediation of CR and NB was also assessed. During the sorption experiments, aliquots of the simulated polluted water samples were collected from the reaction system at 15 min intervals. The experiments revealed that at the optimum NZS-D dosage, the CR and NB remediation was approximately 91 and 90% within 15 min and reached equilibrium at 60 min. In the early stage of the sorption process, the higher abundance of active sites on the surface of NZS-D might have facilitated the high removal of dye molecules. As time progressed, the sorption sites became increasingly occupied, by the dye molecules, and a substantially lower number of vacant sites were available for interaction with dye molecules. Consequently, the rate of adsorption decreased significantly over time. The assessment of the contact time effect was performed at neutral pH and 303 K and the findings, from this investigation, provide valuable insights into the dynamics of CR and NB dye remediation under specific experimental conditions.

The impact of variation of solution pH on the dye adsorption was also examined. Investigation of the effect of pH on sorption was carried out using a dye solution with a 20 mg L^{-1} concentration, a 1.0 g L^{-1} dosage of NZS-D, and a batch volume of 10 mL. The sorption experiments were carried out in a water bath shaker at 120 rpm and 30 °C. The pH of the dye solutions was adjusted to pH range 3–10 by adding 1 N HCl or 1 N NaOH solution, and spectrophotometric analysis was conducted to examine any change in λ_{max} value. The investigation revealed that increasing pH of NB solution did not alter the percentage sorption, specifically, it only increased from 93 to 95%, with maximum removal observed at pH 7, therefore, throughout the experiments, NB solution was maintained at pH 7. In contrast, the solution pH showed a substantial effect on the efficiency of CR removal, which increased from 85 to 97% as the pH decreased from 10 to 3, with maximum removal in the pH range of 4–6. Consequently, the CR solution was maintained at pH 6 for further experiments.

2.6 Statistical error analysis of the adsorption process

The results obtained from the adsorption isotherms and kinetics were analyzed through calculation of the Chi-squared (χ^2) and sum of square error (SSE) values. These two tests were utilized to confirm the best fitting of models, namely, the Langmuir and the Freundlich isotherms and pseudo-first order and pseudo-second order kinetic models. The best-fitting isotherm and kinetic models should have higher regression coefficients and minimum χ^2 and SSE values. The statistical error factor χ^2 and SSE were evaluated using the following relationships:[48]

$$\chi^2 = \sum_{i=1}^{n} \frac{(Q_m(\text{exp.}) - Q_m(\text{cal.}))^2}{Q_m(\text{cal.})}$$

$$\text{SSE} = \sum_{i=1}^{n} (Q_m(\text{exp.}) - Q_m(\text{cal.}))^2$$

The Chi-squared test and SSE values have been discussed herein in respect of isotherm and kinetics modelling.

3. Results and discussion

3.1 Mechanism of the preparation of NZS-D

The goal of developing a cost-effective material, for water treatment, was achieved by preparing NZS-D, which possesses excellent biocompatibility, following a published method with certain modifications.[25] The various phytochemicals of date seed interacted with Ni^{2+} and Zn^{2+} ions, and in the presence of thioacetamide, led to the formation of binary metal sulphide nanoparticles on the grains in a straightforward single-step process, resulting in an organic–inorganic hybrid nanocomposite.[26] The synthesis of the binary metal sulphide was achieved by the addition of NaOH solution, which resulted in the precipitation of the binary metal sulphide.[27,28] Following this, the as-synthesized nanocomposite grains were effectively

separated using centrifugation and washed with deionized water and finally, dried in an oven at 70 °C for 24 h.

The mechanism of formation of the material was rationalized as follows. Initially, the abundant functional groups on the date seed grain (D–OH/D–COOH) might have served as attractive sites for the adsorption of Ni^{2+} and Zn^{2+} ions, leading to their bonding interaction. Subsequently, co-precipitation reactions were initiated, and the significant concentration of NaOH, employed during the reaction, provided a substantial number of OH^- ions on the surface, which further facilitated attraction of the Ni^{2+} and Zn^{2+} towards the date seed grains. The high pH of the solution might has been responsible for the fast nucleation and resulting formation of bimetallic sulphide nanoparticles.[28] It is conceivable that extract from the date powder might has served as a capping agent during the nanoparticle growth by protecting the surface of the binary metal sulphide to produce smaller particles through preventing nanoparticle aggregation.[26] Comprehensive investigation of the surface composition, crystallinity, morphology, particle size, stability and presence of functional groups of the synthesized NZS-D nanomaterial was undertaken using characterization techniques including P-XRD, SEM, EDS, TGA, TEM, and FT-IR.

FT-IR is a valuable analytical technique which was used for elucidating the presence and characteristics of functional groups, bond vibrations, and stretching modes on the surface of the synthesized NZS-D. The spectrum, of NZS-D, exhibited distinct IR absorption peaks attributed to the presence of date grain and bimetallic sulphide particles, which contain different functional groups at the surface. The FT-IR spectrum showed a sharp, low-intensity, peak at 3650 cm^{-1} and wide absorption peaks around 3350 cm^{-1}, corresponding to the hydroxyl groups on the cellulosic part of the seed grains (Fig. 1).[29] The notable peaks at 2940 and 2860 cm^{-1} could be associated with $-CH_3$ and $-CH_2$ group stretching vibrations, respectively.[29] The presence of –C(O)O–, which might be due to carboxyl groups in the date grain–metal sulphide structure, was indicated by the peak at 2372 cm^{-1}.[30] The protein content of the seed grain was apparent from the peaks at 1640 and 1540 cm^{-1}, which corresponded to the amide I and II groups, respectively.[31] Moreover, the composite sample demonstrated IR peaks at 1430, 1270, and 1030 cm^{-1}, in agreement with –OH in-plane bending and C–O stretching vibrations due to the lignocellulosic material of the seed grain and C–O stretching of carboxylic, ester, and ether groups present in cellulose or hemicellulose, respectively.[32] The peaks in the range of 725–930 cm^{-1} might be due to C–H out-of-plane bending vibrations, which are characteristic of long-chain alkanes or out-of-plane C–H bending in aromatic rings in the NZS-D. The IR band in the 600–700 cm^{-1} range indicated Zn–S or Ni–S bond vibrations in the bimetallic sulphide nanoparticles (Fig. 1).[33] Moreover, this peak might also correspond to C–S stretching vibrations because of the organic–sulphur bond formed during nanoparticle synthesis on the date grains. These functional groups on the date seed grains played a vital role in facilitating the formation of metal sulphide nanoparticles on the seed grain surface. Thus, the IR spectrum of the NZS-D exhibited distinct peaks associated with the inherent functional groups of date seed grains, along with vibrations characteristic of bimetallic sulphide, indicating the presence of Ni–Zn–S nanoparticles.

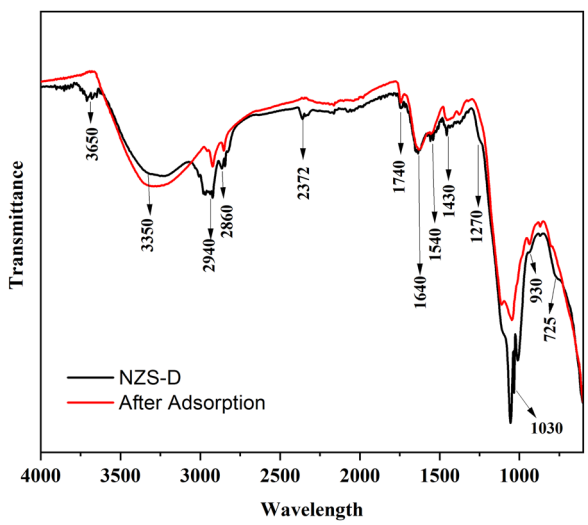

Fig. 1 FT-IR spectrum of NZS-D before and after adsorption of CR.

The various functional groups on the NZS-D surface contribute to its suitability for pollutant adsorption. The IR spectrum of NZS-D after CR adsorption was examined in order to understand the role of various functional groups. The results indicated remarkable shifts in the wavenumbers of certain absorption peaks following adsorption. Specifically, the peak around 3650 cm^{-1} attributed to hydroxyl groups nearly disappeared after adsorption. Similarly, the peak assigned to –OH in-plane bending (1270 cm^{-1}) became almost indistinguishable after CR adsorption. These spectral alterations after CR adsorption provided evidence of interaction between the functional groups of NZS-D and the CR molecules.

FE-SEM imaging, another essential technique for visualizing surfaces at the sub-microscopic scale, offered crucial insights into material topography, crystal shape, and structural characteristics. SEM imaging of NZS-D (Fig. 2a and b) was employed to confirm the growth of Ni–Zn–S nanoparticles at the seed grain surface. The SEM images revealed the rough and quasi-spherical shape of NZS-D due to the agglomeration of bimetallic sulphide nanoparticles. The images also revealed the porous nature of the NZS-D.

EDX analysis of the NZS-D (Fig. 2c) confirmed the presence of carbon, nitrogen and oxygen, nickel, zinc, and sulphur at the surface. The presence of carbon, oxygen, and nitrogen was attributed to the date grain having various functional groups, as indicated by FT-IR analysis. Conversely, the elements nickel, zinc, and sulphur originated from the formation of binary metal sulphide nanoparticles at the surface of date grains. This observation confirmed the successful integration of bimetallic sulphide nanoparticles within the carbon framework of the date seed grain, validating the formation of the NZS-D.

TEM imaging, one of the most effective techniques for examining the dimensions of solid particles at the nanoscale,

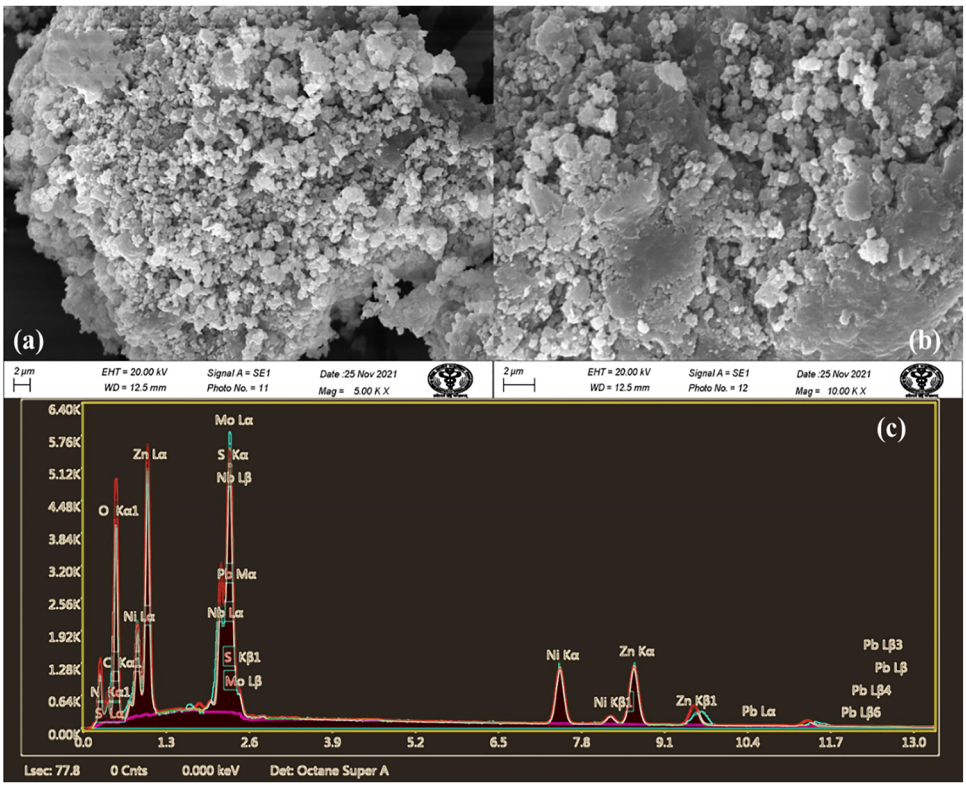

Fig. 2 (a) and (b) SEM images and (c) EDX spectra of NZS-D.

visually demonstrated the development of quasi-spherical nanoparticles on the carbon framework of the date seed grains (Fig. 3a). The presence of nanoparticle agglomeration was also discernible within the TEM image, further indicating the effective growth of metal sulphide nanoparticles on the carbon framework of the date grain. Furthermore, the binary metal sulphide particle sizes were analyzed and histogram was drawn, using ImageJ software, from the TEM images which showed the particle size distribution in the range 70–90 nm.

Thermal stability assessment of the synthesized NZS-D was carried out through TGA analysis by subjecting the composite material to heating over the temperature range of 30–900 °C with an incremental heating rate of 10 °C min^{-1} (Fig. 4). The TGA plot exhibited the distinct degradation of the NZS-D with three prominent stages. The initial degradation phase spanned from 95 °C to approximately 200 °C, in which the weight remained nearly unchanged, *i.e.*, 95%, with only 5% weight loss. The DTA plot showed a small dip in this temperature range, indicating the minor loss of adsorbed moisture or volatile materials *via* endothermic evaporation from NZS-D surface.[34] A second degradation phase occurred between 200 and 500 °C, during which the weight decreased gradually from

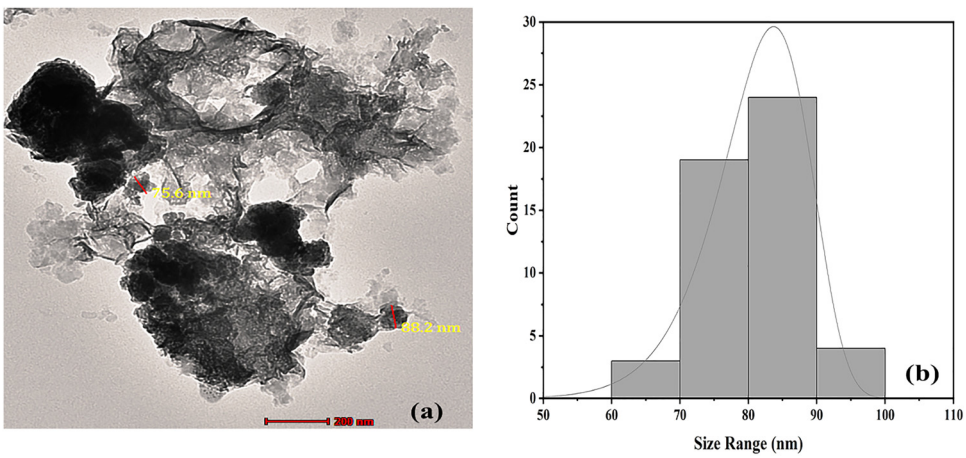

Fig. 3 (a) TEM micrograph of NZS-D. (b) Size distribution histogram.

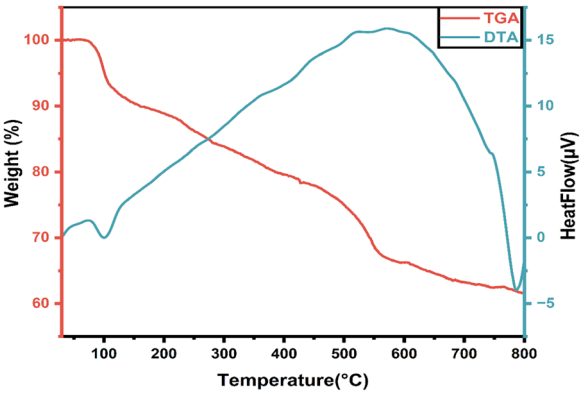

Fig. 4 TGA and DSC plots of NZS-D.

95 to 85%. The DTA plot showed a broad exothermic peak starting at 200 °C and peaking around 400–500 °C. This indicated the combustion of carbonaceous residues, specifically cellulose, hemicellulose, lignin and other principal constituents of NZS-D.[35] At around 550 °C, a major weight loss from ~85 to ~60–65% occurred, and the DTA peak reached its maximum value and then declined sharply, indicating the thermal breakdown of NZS-D. The final decomposition stage occurred at approximately 600–700 °C and above, with the weight stabilization at around 60% corresponding to the remaining inorganic compound. The DTA line dropped, indicating endothermic sublimation of the NZS-D matrix.[36] The TGA analysis demonstrated that NZS-D possessed excellent thermal stability and maintained its integrity up to 750 °C. This level of stability suggests that the material can perform effectively in real-world high-temperature applications.

The P-XRD pattern of the NZS-D (Fig. 5) showed discernible peaks at 30.66, 46.48, and 54.84° (2θ), which corresponded to Miller planes (111), (220), and (311) of NiS and ZnS nanoparticles, respectively (JCPDS File No. 65-4586).[37] Furthermore, the peaks observed at 38.88 and 60.68° could be attributed to the presence of NiS, aligning with (220) and (012) planes, respectively.[38,39] This angular data unequivocally confirmed

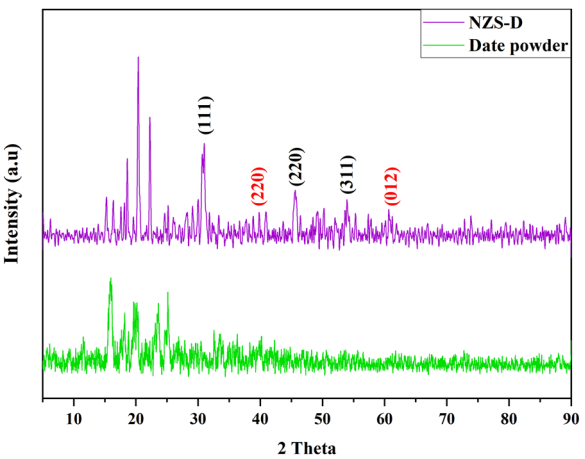

Fig. 5 X-ray diffraction pattern of the synthesised NZS-D.

the composite nature of the NZS-D with bimetallic sulphide encompassing both Ni and Zn. An XRD investigation of the pristine seed grains was additionally conducted (depicted in the green spectrum) for comparison. Examination of the XRD patterns highlighted the emergence of new peaks subsequent to the synthesis of the NZS-D, unequivocally confirming the successful formation of bimetallic sulphide integrated into the carbon framework of the seed grains. Furthermore, there is a noticeable reduction in the intensity of the peaks of the pristine date grains after the formation of the composite. This distinct alteration unequivocally signified the successful creation of NZS-D.

3.2 Role of temperature, thermodynamics and isotherms

The influence of temperature on the sorption capability of NZS-D was investigated. The experimental findings revealed a decline in the sorption capacity of NZS-D, for CR and NB, with increasing temperature which is consistent with observations reported by others.[40] This behaviour might be attributed to the crucial role of the functional groups present on NZS-D surface, which served as the driving force for the sorption process.[41] As the temperature increased, the bonds between NZS-D and dye molecules might have weakened, leading to the escape of dye molecules from binding sites and hence a reduction in adsorption efficiency. Furthermore, at elevated temperatures, the kinetic energy of CR and NB molecules might have increased, hindering the possibility of strong interactions between these molecules and the functional groups of the NZS-D.

Furthermore, the investigation was extended to ascertain the thermodynamic parameters of the sorption process, and the viability of NB and CR sorption was predicted from the sign and magnitude of the Gibbs free energy, ΔG, enthalpy, ΔH, and entropy, ΔS (Table 1).[13] The enthalpy change was found negative for the sorption of NB, suggesting an exothermic reaction, whereas it was positive for CR, suggesting an endothermic nature. The entropy change was also determined and found to be positive for the adsorption of both NB and CR, which indicated an increase in randomness at the interface of the solid and the aqueous medium.

The feasibility of the present sorption process, at various temperatures, was investigated through calculation of Gibbs free energy. The numerical values of ΔG at three temperatures were found consistently negative (Table 1), suggesting the sorption of NB and CR onto NZS-D a feasible and spontaneous phenomenon in the tested temperature range.

Table 1 Thermodynamic parameters for the adsorption of the dyes CR and NB onto NZS-D

Pollutants	Temperature (K)	ΔG (kJ mol^{-1})	ΔH (kJ mol^{-1})	ΔS (kJ mol^{-1} K^{-1})
NB	303	−4.966	−0.512	0.015
	313	−5.113		
	323	−5.260		
CR	303	−0.138	19.496	0.065
	313	−0.786		
	323	−1.434		

The adsorption experiments were performed at 303, 313 and 323 K while maintaining the optimum concentration, dosage, and contact time. The observed reduction in the percentage adsorption with increasing temperature suggested an endothermic nature of the sorption phenomenon for both CR and NB. Subsequently, the collected sorption data were analyzed by substituting in the Langmuir, Freundlich, and Temkin isotherms, and the pertinent parameters were calculated to determine a probable mechanism of interaction between NZS-D and the CR and NB molecules. The Langmuir and the Freundlich isotherms are given by eqn (3) and (4), respectively:[42,43]

$$\frac{C_e}{Q_e} = \frac{C_e}{Q_0} + \frac{1}{Q_0 K_L} \quad (3)$$

$$\log Q_e = \log k_F + \frac{1}{n}\log C_e \quad (4)$$

In the present context, the equilibrium sorption capacity of NZS-D, denoted as Q_e (mg g^{-1}), is correlated with the dye concentration at equilibrium, C_e (mg L^{-1}). The Langmuir constant K_L (L mg^{-1}), is an indicator of the binding energy between the dye and NZS-D. The maximum sorption capacity of NZS-D for CR or NB sorption is denoted as Q_m (mg g^{-1}). The Freundlich isotherm, which is based on the concept of a pollutant adsorbing onto a heterogeneous surface, describes the attachment of CR or NB to sites with varying binding affinities.[44] The parameters k_F and n represent the degree of pollutant adsorption capacity of the NZS-D and intensity when the concentration is at a unit level. The Langmuir isotherm is built upon the idea that pollutants form a monolayer on a uniformly energetic surface, and assumes that the dye ions are evenly spread across a surface with nearly identical affinities for the CR or NB dye molecules.[45,46]

In parallel with the aforementioned isotherms, the Temkin isotherm, whose formula is given below, includes a component that describes the interaction between the solid and the pollutant as a chemical bond. The derivation of the Temkin isotherm takes into consideration the heat of sorption, which decreases linearly with the coverage of the solid surface rather than exhibiting an exponential decrease as surface coverage increases.[47]

$$Q_e = \frac{RT}{b_T}\ln A_T + \frac{RT}{b_T}\ln C_e \quad (5)$$

Here, b_T is a constant corresponding to the heat of sorption (J mol^{-1}), and A_T is a constant that is a measure of the binding energy (L g^{-1}).

The regression coefficients, Chi-squared (χ^2), and sum of square error (SSE), of the values obtained from the plots were used to validate the fitting of the sorption data to the Temkin, Freundlich and Langmuir isotherms. The slope and intercept of the plots provided the values of various process parameters, which were exploited to propose a mechanism for the sorption of the dyes CR and NB onto the surface of NZS-D.

Freundlich isotherm plots (Fig. 7) exhibited correlation coefficients of 0.999 in the investigated temperature range, signifying the good fit of the adsorption data to the Freundlich isotherm. This fitting implied that NZS-D possessed a non-homogeneous surface. The value of the heterogeneity factor (n) was found greater than unity, suggesting a physisorption phenomenon and a relatively heterogeneous nature of the NZS-D surface. The isotherm plots have the highest R^2 values and minimum χ^2 value.[48]

However, the regression coefficients for the Langmuir isotherm plots (Fig. 6) were also found nearly unity, which suggested that the sorption system might follow both these isotherms. The observation that the sorption system was consistent with both Langmuir and Freundlich isotherms revealed that the solid surface might be partially homogeneous and partially heterogeneous, and that bonding between the dyes and NZS-D might occurred through specific functional groups. In the lower concentration range, used in the present sorption system, the experimental sorption data might not challenge the differences between the two models significantly.[49] However, the sorption capacities of the NZS-D for CR and NB have been compared based on the Langmuir parameters only. The results indicated a variation in the sorption capacity of NZS-D for CR, with a higher sorption capacity of 208.333 mg g^{-1}, as

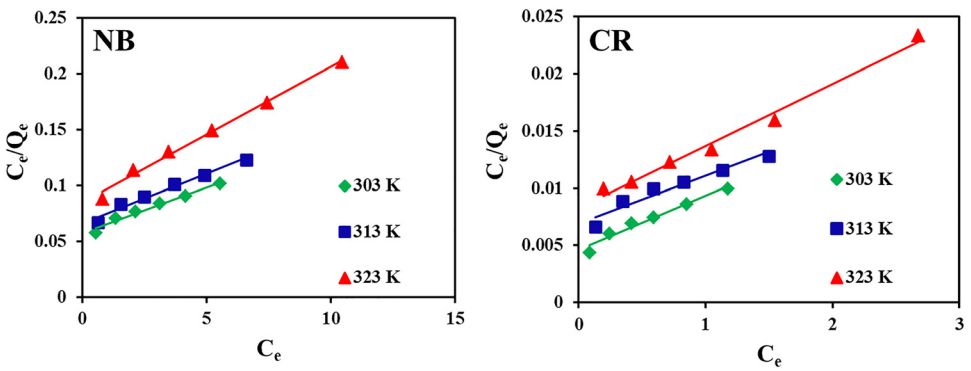

Fig. 6 Langmuir isotherms for NB and CR at 303, 313 and 323 K.

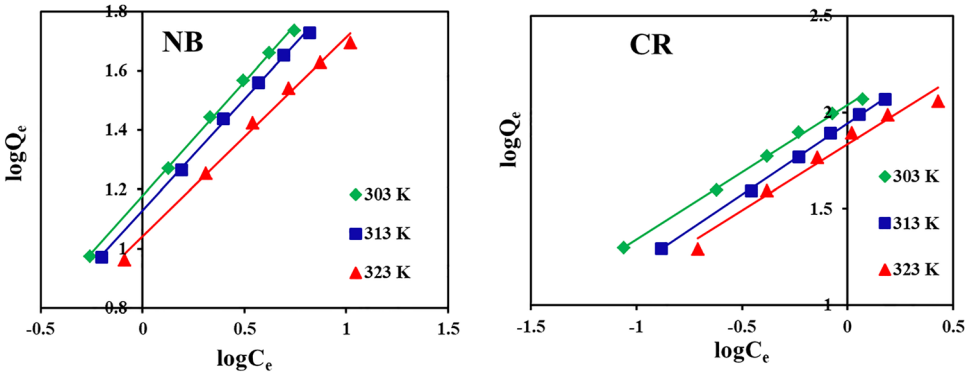

Fig. 7 Freundlich isotherms for NB and CR at 303, 313 and 323 K.

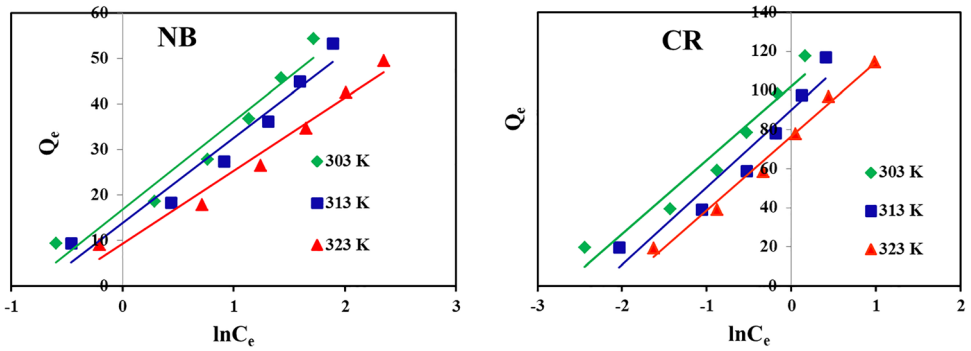

Fig. 8 Temkin isotherms for NB and CR at 303, 313 and 323 K.

compared to that for NB, with a maximum sorption capacity of 121.951 mg g^{-1}.

The Temkin isotherm (Fig. 8) constants A_T and b_T denote binding energy and heat of sorption, respectively. The A_T values, for the dyes CR and NB, decreased with increasing temperature, suggesting reduced sorption at elevated temperature. CR exhibited a higher A_T value than NB, indicating a higher binding energy or greater sorption probability. These observations further reinforced the sorption capacity predictions made based on the Langmuir isotherm analysis (Table 2).[50]

Table 2 Langmuir, Freundlich, and Temkin isotherm parameters for the dyes CR and NB at 303 K

Model	Parameter	CR (anionic dye)	NB (cationic dye)
Langmuir	Q_m (mg g^{-1})	208.333	121.951
	K_L (L mg^{-1})	0.087	0.413
	R_L^2	0.963	0.973
	χ^2	0.424	0.068
	SSE	26.878	2.058
Freundlich	K_F (L mg^{-1})	109.194	15.111
	n_F	1.434	1.301
	R_F^2	0.999	0.926
	χ^2	0.351	0.109
	SSE	33.787	5.246
Temkin	A_T	15.021	2.370
	b_T	37.701	19.491
	R_T^2	0.945	0.949

3.3 Adsorption kinetics

The effect of contact time on the performance of NZS-D, for CR and NB adsorption, was investigated. The assessment of the sorption capacity and efficiency over time provided valuable insights into the kinetics for the specific pollutants, enabling the proposal of the underlying mechanism governing the sorption process. The investigation of sorption kinetics was conducted at a concentration of 20 mg L^{-1} and a temperature of 303 K for both CR and NB, with a dosage of 0.5 g L^{-1} for CR and 1.0 g L^{-1} for NB. The pseudo-first order (PFO) and pseudo-second order (PSO) models given below (eqn (6) and (7)) were used to analyze the adsorption kinetics data:[51]

$$\log(Q_e - Q_t) = \log Q_e - \frac{k_1}{2.303}t \quad (6)$$

$$\frac{t}{Q_t} = \frac{1}{h} + \frac{t}{Q_e} \quad (7)$$

In the present context, the symbol Q_t (mg g^{-1}) denotes the NZS-D adsorption capacity at time t, while k_1 (min^{-1}) represents the rate constant associated with the PFO kinetics and k_2 (g mg^{-1} min^{-1}) pertains to the rate constant for the PSO kinetics. By employing the aforementioned correlations, the relevant parameters, for both dyes, were determined (Table 3).

For NZS-D, the PSO plots exhibited strong agreement with the theoretical and experimental adsorption capacities, and the

Table 3 Kinetic parameters obtained from the PFO and PSO kinetic models

		PFO					PSO				
Dye	Q_e, exp mg g^{-1}	Q_e, cal mg g^{-1}	K_1 min^{-1}	R^2	Chi square	SSE	Q_e, cal mg g^{-1}	K_2 g mg^{-1} min^{-1}	R^2	Chi square	SSE
CR	39.695	7.244	0.041	0.938	145.366	1053.083	40.650	0.011	1	0.022	0.912
NB	19.136	3.663	0.070	0.910	65.347	239.4	19.379	0.048	1	0.003	0.059

regression coefficients were almost unity, which suggested that the PSO model was the most suitable choice for the investigation of the kinetics of the sorption of CR and NB (Table 3). Moreover, the low χ^2 and SSE values revealed that the PSO kinetics model fitted the sorption data better for the adsorption of both CR and NB.[48] The better fitting of the sorption data to PSO model implied that the primary factors which influenced the adsorption process were dosage of NZS-D and concentration of the CR and NB in water. Furthermore, for the PSO, the rate constant k_2 was determined to be lower than that for the PFO model, further confirming that the CR and NB sorption process adhered to the PSO kinetic model.[52,53]

3.4 Mechanism of adsorption

An in-depth investigation was undertaken to comprehend the mechanism of the adsorption of CR and NB onto NZS-D surface (Fig. 9). Various aspects, such as the surface heterogeneity, surface roughness, and solution pH data, were employed to propose the sorption mechanism. The obtained sorption data were exploited to identify the types of forces between the NZS-D surface and CR and NB, *i.e.*, electrostatic or Van der Waals forces and coordination bonding. Initially, the only considerations were the potential role of the surface and Van der Waals interactions, but these factors alone could not explain the selective adsorption of CR and NB with high efficacy. Coordination bonding was excluded because no significant shifts in peaks in the FT-IR spectra were observed after dye adsorption onto the NZS-D surface. Consequently, Van der Waals forces or electrostatic interaction emerged as the pivotal determinants which were substantiated by the investigation of pH effect on the dye adsorption. At lower pH levels, a slight decrease in CR adsorption was observed, likely due to protonation of the CR molecules which reduced their anionic character or constantly competed with the H^+ ions for functional sites on the protonated NZS-D surface.

Furthermore, the zeta potential of NZS-D was found −12.66 mV which confirmed the negative charge on the surface. The surface charge of NZS-D played a pivotal role in fostering electrostatic interactions with the anionic CR ions at lower pH. The percentage removal demonstrated a decline under highly acidic conditions due to the binding of the protonated CR molecules through the unshared electron pairs of the nitrogen atoms with protonated NZS-D surface which caused repulsion by the increasing concentration of H^+ ions in the solution.[54] Therefore, a competitive environment was created between the H^+ ions and the CR molecules for adsorption on the NZS-D surface, and consequently, the percentage removal decreased. Upon increasing the pH to 6, the H^+ ions were neutralised and the CR molecules thus had enough space to be adsorbed on the NZS-D surface.[55] Above neutral pH, the CR molecules transitioned to an anionic state, augmenting the electrostatic repulsion, which resulted in a lowering of the percentage adsorption.

A similar electrostatic interaction was also observed with the NB molecules. The highest uptake was observed at pH 7, and the adsorption became saturated thereafter. This phenomenon

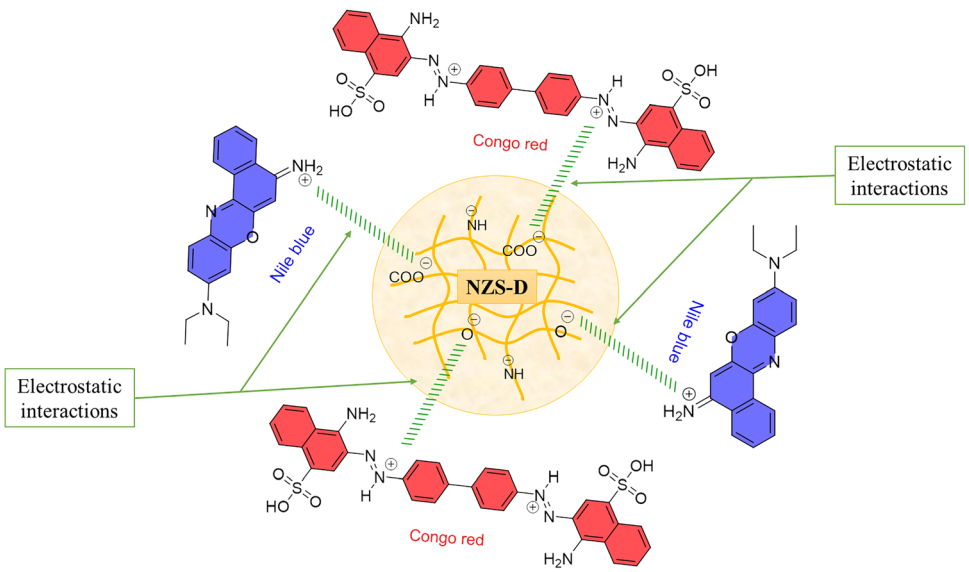

Fig. 9 Plausible mechanism of CR and NB adsorption onto the NZS-D surface.

Table 4 A comparative study of various sorbents used for the elimination of the dye CR

Sorbent	Dose (g L^{-1})	Temperature (K)	pH	Q_{max} (mg g^{-1})	Ref.
$ZnFe_2O_4/SiO_2$/tragacanth gum	0.2	—	5	159.90	57
Chitosan/montmorillonite nanocomposite	4.0	323	7	54.52	58
$FeNi_3/SiO_2/CuS$	1.0	323	5	42.73	59
Fe_3O_4@graphene	0.4	—	10	33.66	60
Alginate/γ-Fe_2O_3/CdS	0.5	—	—	20.31	61
Chitosan-coated magnetic Fe_3O_4 nanocomposite	—	—	—	1.8257	62
L-Cys/rGO/PANI	—	333	7	56.57	63
Magnetic cellulose/Fe_3O_4/activated carbon	—	298	4	66.09	64
Au–Fe_3O_4–AC	—	—	4	43.88	65
N,*O*-Carboxymethyl-chitosan/montmorillonite	—	323	7	74.24	66
SiO_2 nanoparticle	0.5	—	4	22.4	67
NZS-D	0.5	303	4–6	208.333	This work

might be ascribed, in part, to the prevalence of negatively charged sites on the NZS-D and a relatively higher abundance of H^+ ions in the solution, thereby causing electrostatic competition between the H^+ ions and NB molecules at lower pH values. As the pH was increased, the H^+ ion concentration decreased, and no positive species other than the NB molecule were present, facilitating an augmentation of negatively charged sites that might have attracted the positively charged NB molecules.[56] This phenomenon was observed up to neutral pH and became almost constant thereafter.

In conclusion, the intricate interplay of electrostatic interactions among the negatively charged surface of NZS-D and the anionic CR and cationic NB molecules served as the driving force for their selective and efficient adsorption, as substantiated by the pH-dependent variations in adsorption efficacy. This electrostatically mediated adsorption phenomenon holds significant implications for optimizing dye removal processes in water treatment applications.

3.5 Comparative study of adsorption based on prior literature data

A comparison of different adsorbents has been made based on their efficiency for the removal of dyes under various conditions. Comparisons of NZS-D with other materials in the literature, in terms of sorption capacity, for CR and NB dyes, is given in Tables 4 and 5. This comparative study demonstrated that NZS-D outperformed the previously reported materials.

Table 5 A comparative study of various sorbents used for the elimination of the dye NB

Sorbent	Dose (g L^{-1})	Temperature (K)	pH	Q_{max} (mg g^{-1})	Ref.
$AC/CoFe_2O_4$	—	—	8	86.24	68
$CuWO_4$	4.0	—	10	1.069	69
Activated carbon	0.5	—	7	27	70
Graphene oxide	—	—	7	50	
Guava leaf powder (GLP)	0.5	—	—	14.85	71
Fe_3O_4@P(MMA-*co*-GMA)	—	—	—	109.4	72
Hydroxyapatite@Mn–Fe	1.0	298	10	91.36	73
$CNT/MgO/CuFe_2O_4$	1.0	298	8	35.60	74
Ferrofluid-modified sawdust	—	—	9.2	51.093	75
Clay/starch/$MnFe_2O_4$	—	—		72.25	76
NZS-D	0.5	303	4–6	121.951	This work

Conclusion

In this work, a facile co-precipitation technique was employed for the development of the composite NZS-D, as a potential material for the sorptive elimination of the dyes, Congo red and Nile blue, from water. The synthesized NZS-D has been comprehensively characterized through IR, XRD, SEM, EDX, TGA and TEM techniques which revealed the porous structure with abundant functional sites on the surface. TEM imaging has demonstrated the size distribution of NZS-D particles in the ranged 70–90 nm. The adsorption investigation unveiled the remarkable efficacy of the NZS-D with sorption capacities, computed from the Langmuir isotherm, of 208.333 mg g^{-1} for Congo red and 121.951 mg g^{-1} for Nile blue at 303 K. The sorption data fitting analysis followed the Freundlich isotherm, suggesting physical sorption of dyes on the NZS-D surface, which could be attributed to the electrostatic interaction between the surface functional groups and Nile blue and Congo red molecules. The findings of this study underscore the efficacy of the NZS-D composite as a proficient material for wastewater treatment *via* adsorption technology. However, pilot-scale adsorption evaluation using real industrial wastewater is essential to validate the practical applicability of the developed material. For future prospects, other materials may be explored for sustainable development.[77–79]

Author contributions

Conceived and designed the experiments: Saif Ali Chaudhry, Mohammed K. Al Mesfer, Mohd Danish; formal analysis and data curation: Md. Sajid, Atul Sharma; Original draft writing: Md. Sajid, Atul Sharma; Writing – reviewing and editing: Saif Ali Chaudhry, Mohammed K. Al Mesfer, Mohd Danish; and Supervision and project administration: Saif Ali Chaudhry. All authors have read and agreed to publish the manuscript.

Conflicts of interest

All authors state that they do not have any recognized financial or personal conflicts that might seem to influence the findings presented in this study.

Data availability

The authors confirm that the data supporting the findings of the study are available within the article.

Acknowledgements

The authors extend their appreciation to the University Higher Education Fund, Saudi Arabia, for funding this research work under Research Support Program for Central labs., King Khalid University, Saudi Arabia, through the Project No. CL/CO/B/6.

References

1 X. Li, M. Zhou, J. Jia and Q. Jia, A water-insoluble viologen-based β-cyclodextrinpolymer for selective adsorption toward anionic dyes, *React. Funct. Polym.*, 2018, **126**, 20–26, DOI: 10.1016/j.reactfunctpolym.2018.03.004.

2 M. Sajid, A. Sharma and S. A. Chaudhry, Environmental remediation through bimetallic sulphide-derived adsorbents: Prospects and progress, *Chem. Eng. Res. Des.*, 2024, **203**, 651–662, DOI: 10.1016/j.cherd.2024.01.052.

3 T. Shindhal, P. Rakholiya, S. Varjani, A. Pandey, H. H. Ngo, W. Guo, H. Y. Ng and M. J. Taherzadeh, A critical review on advances in the practices and perspectives for the treatment of dye industry wastewater, *Bioengineered*, 2020, **12**, 70–87, DOI: 10.1080/21655979.2020.1863034.

4 S. Rangabhashiyam, N. Anu and N. Selvaraju, Sequestration of dye from textile industry wastewater using agricultural waste products as adsorbents, *J. Environ. Chem. Eng.*, 2013, **1**(4), 629–641, DOI: 10.1016/j.jece.2013.07.014.

5 M. Sajid, A. Sharma, S. Shukla, A. Khan and S. Ali Chaudhry, Nano-Enhanced Water purification: Uncovering the dye adsorption efficiency of NiZnS@Cyclodextrine Nanomaterial, *ChemistrySelect*, 2024, **9**(33), e202400093, DOI: 10.1002/slct.202400093.

6 K. Naseem, Z. H. Farooqi, R. Begum and A. Irfan, Removal of Congo red dye from aqueous medium by its catalytic reduction using sodium borohydride in the presence of various inorganic nano-catalysts: A review, *J. Cleaner Prod.*, 2018, **187**, 296–307, DOI: 10.1016/j.jclepro.2018.03.209.

7 IARC working group on the evaluation of carcinogenic risks to humans. Chemical agents and related occupations. Lyon (FR): International agency for research on cancer; 2012. (IARC monographs on the evaluation of carcinogenic risks to humans, No. 100F. dyes metabolized to benzidine, https://www.ncbi.nlm.nih.gov/books/NBK304402/ (accessed on 7 March 2023).

8 S. Dutta, B. Gupta, S. K. Srivastava and A. K. Gupta, Recent advances on the removal of dyes from wastewater using various adsorbents: A critical review, *Mater. Adv.*, 2021, **2**(14), 4497–4531, DOI: 10.1039/D1MA00354B.

9 K. Sathishkumar, M. S. AlSalhi, E. Sanganyado, S. Devanesan, A. Arulprakash and A. Rajasekar, Sequential electrochemical oxidation and bio-treatment of the azo dye congo red and textile effluent, *J. Photochem. Photobiol., B*, 2019, **200**, 111655, DOI: 10.1016/j.jphotobiol.2019.111655.

10 P. C. Nnaji, V. C. Anadebe, I. G. Ezemagu and O. D. Onukwuli, Potential of Luffa cylindrica seed as coagulation-flocculation (CF) agent for the treatment of dye wastewater: kinetic, mass transfer, optimization and CF adsorption studies, *Arabian J. Chem.*, 2022, **15**(2), 103629, DOI: 10.1016/j.arabjc.2021.103629.

11 L. Z. Huang, H. C. B. Hansen and M. J. Bjerrum, Electrochemical reduction of nitroaromatic compounds by single sheet iron oxide coated electrodes, *J. Hazard. Mater.*, 2016, **306**, 175–183, DOI: 10.1016/j.jhazmat.2015.12.009.

12 N. Abbasi, S. A. Khan and T. A. Khan, Response surface methodology mediated process optimization of Celestine blue B uptake by novel custard apple seeds activated carbon/$FeMoO_4$ nanocomposite, *J. Water Process Eng.*, 2021, **43**, 102267, DOI: 10.1016/j.jwpe.2021.102267.

13 A. Sharma, D. Mangla, A. Choudhry, M. Sajid and S. A. Chaudhry, Facile synthesis, physico-chemical studies of Ocimum sanctum magnetic nanocomposite and its adsorptive application against Methylene blue, *J. Mol. Liq.*, 2022, **362**, 119752, DOI: 10.1016/j.molliq.2022.119752.

14 L. Liu, Z. Chen, J. Zhang, D. Shan, Y. Wu, L. Bai and B. Wang, Treatment of industrial dye wastewater and pharmaceutical residue wastewater by advanced oxidation processes and its combination with nanocatalysts: A review, *J. Water Process Eng.*, 2021, **42**, 102122, DOI: 10.1016/j.jwpe.2021.102122.

15 A. Shahzaib, I. Ahmad, P. Singh, F. Zafar, Y. Akhtar, A. A. Bukhari and N. Nishat, Ultrarapid and highly efficient reduction of nitroaromatic compounds using cyclodextrin MOF, *Catal. Commun.*, 2023, **174**, 106569, DOI: 10.1016/j.catcom.2022.106569.

16 A. Shahzaib, Shaily, I. Ahmad, F. Zafar, S. M. Alshehri, S. Ali and N. Nishat, One pot synthesis of cyclodextrin MOF as a promising heterogeneous catalyst for the reduction of nitroaromatic compounds and azo dyes, *Res. Chem. Intermed.*, 2023, **49**(6), 2507–2528, DOI: 10.1007/s11164-023-04986-9.

17 U. W. Siagian, A. Raksajati, N. F. Himma, K. Khoiruddin and I. G. Wenten, Membrane-based carbon capture technologies: Membrane gas separation *vs.* membrane contactor, *J. Nat. Gas Sci. Eng.*, 2019, **67**, 172–195, DOI: 10.1016/j.jngse.2019.04.008.

18 K. F. Ulbrich, E. N. Nishida, B. S. Souza and C. E. M. Campos, NiS_2-NiS nanocrystalline composite synthesized by mechanochemistry and its performance for methylene blue dye adsorption, *Mater. Chem. Phys.*, 2020, **252**, 123226, DOI: 10.1016/j.matchemphys.2020.123226.

19 A. K. Sharma, B. S. Kaith, V. Tanwar, J. K. Bhatia, N. Sharma, S. Bajaj and S. Panchal, RSM-CCD optimized sodium alginate/gelatin based ZnS-nanocomposite hydrogel for the effective removal of biebrich scarlet and crystal violet dyes, *Int. J. Biol. Macromol.*, 2019, **129**, 214–226, DOI: 10.1016/j.ijbiomac.2019.02.034.

20 A. Chowdhury, A. A. Khan, S. Kumari and S. Hussain, Superadsorbent Ni-Co-S/SDS nanocomposites for ultrahigh

removal of cationic, anionic organic dyes and toxic metal ions: Kinetics, isotherm and adsorption mechanism, *ACS Sustainable Chem. Eng.*, 2019, **7**(4), 4165–4176, DOI: 10.1021/acssuschemeng.8b05775.

21 Z. Mahdi, Q. J. Yu and A. El Hanandeh, Investigation of the kinetics and mechanisms of nickel and copper ions adsorption from aqueous solutions by date seed derived biochar, *J. Environ. Chem. Eng.*, 2018, **6**(1), 1171–1181, DOI: 10.1016/j.jece.2018.01.021.

22 P. Chakraborty, S. D. Singh, I. Gorai, D. Singh, W. U. Rahman and G. Halder, Explication of physically and chemically treated date stone biochar for sorptive remotion of ibuprofen from aqueous solution, *J. Water Process Eng.*, 2020, **33**, 101022, DOI: 10.1016/j.jwpe.2019.101022.

23 J. Zhao, Z. Lu, X. He, X. Zhang, Q. Li, T. Xia and C. Lu, Fabrication and characterization of highly porous Fe(OH)3@ cellulose hybrid fibers for effective removal of Congo red from contaminated water, *ACS Sustainable Chem. Eng.*, 2017, **5**(9), 7723–7732, DOI: 10.1021/acssuschemeng.7b01175.

24 S. Kumari, A. A. Khan, A. Chowdhury, A. K. Bhakta, Z. Mekhalif and S. Hussain, Efficient and highly selective adsorption of cationic dyes and removal of ciprofloxacin antibiotic by surface modified nickel sulfide nanomaterials: Kinetics, isotherm and adsorption mechanism, *Colloids Surf., A*, 2020, **586**, 124264, DOI: 10.1016/j.colsurfa.2019.124264.

25 M. S. Podder and C. B. Majumder, Bacteria immobilization on neem leaves/$MnFe_2O_4$ composite surface for removal of As(III) and As(V) from wastewater, *Arabian J. Chem.*, 2019, **12**(8), 3263–3288, DOI: 10.1016/j.arabjc.2015.08.025.

26 S. Saif, A. Tahir and Y. Chen, Green synthesis of iron nanoparticles and their environmental applications and implications, *Nanomaterials*, 2016, **6**(11), 209, DOI: 10.3390/nano6110209.

27 M. Nawaz, Y. Sliman, I. Ercan, M. K. Lima-Tenório, E. T. Tenório-Neto, C. Kaewsaneha and A. Elaissari, Magnetic and pH-responsive magnetic nanocarriers, *Stimuli responsive polymeric Nanocarriers for drug delivery applications*, Woodhead Publishing, 2019, pp. 37–85, DOI: 10.1016/B978-0-08-101995-5.00002-7.

28 A. Rifianto, J. Widakdo, N. Istikhomah, E. Suharyadi, T. Kato and S. Iwata, The effect of synthesis parameter on crystal structure and magnetic properties of $Ni_{0.5}Zn_{0.5}Fe_2O_4$ magnetic nanoparticles, *Journal of Physics: Conference Series*, IOP Publishing, 2018, vol. 1011, no. 1, p. 012059, DOI: 10.1088/1742-6596/1011/1/012059.

29 H. Wang, Q. Yao, C. Wang, B. Fan, Q. Sun, C. Jin and Y. Chen, A simple, one-step hydrothermal approach to durable and robust superparamagnetic, superhydrophobic and electromagnetic wave-absorbing wood, *Sci. Rep.*, 2016, **6**(1), 35549, DOI: 10.1038/srep35549.

30 E. J. Berquist, C. A. Daly Jr, T. Brinzer, K. K. Bullard, Z. M. Campbell, S. A. Corcelli and D. S. Lambrecht, Modeling carbon dioxide vibrational frequencies in ionic liquids: I. Ab initio calculations, *J. Phys. Chem. B*, 2017, **121**(1), 208–220, DOI: 10.1021/acs.jpcb.6b09489.

31 G. Yuvaraja, N. C. Zheng, Y. Pang, M. Su, D. Y. Chen, L. J. Kong and J. C. Wen, Removal of U(VI) from aqueous and polluted water solutions using magnetic Arachis hypogaea leaves powder impregnated into chitosan macromolecule, *Int. J. Biol. Macromol.*, 2020, **148**, 887–897, DOI: 10.1016/j.ijbiomac.2020.01.042.

32 A. Dutta, Fourier transform infrared spectroscopy. *Spectroscopic methods for nanomaterials characterization*, 2017, pp. 73–93., DOI: 10.1016/B978-0-323-46140-5.00004-2.

33 J. M. Baruah, S. Kalita and J. Narayan, Green chemistry synthesis of biocompatible ZnS quantum dots (QDs): Their application as potential thin films and antibacterial agent, *Int. Nano Lett.*, 2019, **9**(2), 149–159, DOI: 10.1007/s40089-019-0270-x.

34 Z. Wang, X. Xiao, T. Zou, Y. Yang, X. Xing, R. Zhao and Y. Wang, Citric acid capped CdS quantum dots for fluorescence detection of copper ions (II) in aqueous solution, *Nanomaterials*, 2018, **9**(1), 32, DOI: 10.3390/nano9010032.

35 I. K. Erabee, A. Ahsan, N. N. N. Daud, S. Idrus, S. Shams, M. F. M. Din and S. Rezania, Manufacture of low-cost activated carbon using sago palm bark and date pits by physiochemical activation, *BioResources*, 2017, **12**(1), 1916–1923, DOI: 10.15376/biores.12.1.1916-1923.

36 M. Sajid, A. Sharma, A. Choudhry and S. A. Chaudhry, Synthesis, characterization and potential application of functionalised binary metallic sulphide for water reclamation, *Colloids Surf., C*, 2023, **1**, 100011, DOI: 10.1016/j.colsuc.2023.100011.

37 N. Priyadharsini, M. Elango, S. Vairam and M. Thamilselvan, Effect of nickel substitution on structural, optical, magnetic properties and photocatalytic activity of ZnS nanoparticles, *Mater. Sci. Semicond. Process.*, 2016, **49**, 68–75, DOI: 10.1016/j.mssp.2016.03.033.

38 H. Geng, S. F. Kong and Y. Wang, NiS nanorod-assembled nanoflowers grown on graphene: morphology evolution and Li-ion storage applications, *J. Mater. Chem. A*, 2014, **2**(36), 15152–15158, DOI: 10.1039/C4TA03440F.

39 Y. Wang, Q. Zhu, L. Tao and X. Su, Controlled-synthesis of NiS hierarchical hollow microspheres with different building blocks and their application in lithium batteries, *J. Mater. Chem.*, 2011, **21**(25), 9248–9254, DOI: 10.1039/C1JM10271K.

40 H. Hosseinzadeh and S. Mohammadi, Quince seed mucilage magnetic nanocomposites as novel bioadsorbents for efficient removal of cationic dyes from aqueous solutions, *Carbohydr. Polym.*, 2015, **134**, 213–221, DOI: 10.1016/j.carbpol.2015.08.008.

41 K. B. Tan, M. Vakili, B. A. Horri, P. E. Poh, A. Z. Abdullah and B. Salamatinia, Adsorption of dyes by nanomaterials: recent developments and adsorption mechanisms, *Sep. Purif. Technol.*, 2015, **150**, 229–242, DOI: 10.1016/j.seppur.2015.07.009.

42 D. Mangla, A. Sharma and S. Ikram, Synthesis of ecological chitosan/PVP magnetic composite: Remediation of amoxicillin trihydrate from its aqueous solution, isotherm modelling, thermodynamic, and kinetic studies, *React. Funct. Polym.*, 2022, **175**, 105261, DOI: 10.1016/j.reactfunctpolym.2022.105261.

43 T. Santhi, S. Manonmani, V. S. Vasantha and Y. T. Chang, A new alternative adsorbent for the removal of cationic dyes

from aqueous solution, *Arabian J. Chem.*, 2016, **9**, S466–S474, DOI: 10.1016/j.arabjc.2011.06.004.

44 M. M. Sadeghi, A. S. Rad, M. Ardjmand and A. Mirabi, Preparation of magnetic nanocomposite based on polyaniline/Fe_3O_4 towards removal of lead(II) ions from real samples, *Synth. Met.*, 2018, **245**, 1–9, DOI: 10.1016/j.synthmet.2018.08.001.

45 S. Rahimi, R. M. Moattari, L. Rajabi, A. A. Derakhshan and M. Keyhani, Iron oxide/hydroxide (α, γ-FeOOH) nanoparticles as high potential adsorbents for lead removal from polluted aquatic media, *J. Ind. Eng. Chem.*, 2015, **23**, 33–43, DOI: 10.1016/j.jiec.2014.07.039.

46 J. H. Deng, X. R. Zhang, G. M. Zeng, J. L. Gong, Q. Y. Niu and J. Liang, Simultaneous removal of Cd(II) and ionic dyes from aqueous solution using magnetic graphene oxide nanocomposite as an adsorbent, *Chem. Eng. J.*, 2013, **226**, 189–200, DOI: 10.1016/j.cej.2013.04.045.

47 D. Ao, L. Ap and O. Am, Langmuir, Freundlich, Temkin and Dubinin–Radushkevich isotherms studies of equilibrium sorption of Zn^{2+} unto phosphoric acid modified rice husk, *IOSR J. Appl. Chem.*, 2012, **3**(1), 38–45, DOI: 10.9790/5736-0313845.

48 B. A. M. Babakir, L. I. A. Ali and H. K. Ismail, Rapid removal of anionic organic dye from contaminated water using a poly(3-aminobenzoic acid/graphene oxide/cobalt ferrite) nanocomposite low-cost adsorbent via adsorption techniques, *Arabian J. Chem.*, 2022, **15**(12), 104318, DOI: 10.1016/j.arabjc.2022.104318.

49 S. Kumar, G. Verma, W. Y. Gao, Z. Niu, L. Wojtas and S. Ma, Anionic metal–organic framework for selective dye removal and CO_2 fixation, *Eur. J. Inorg. Chem.*, 2016, (27), 4373–4377, DOI: 10.1002/ejic.201600218.

50 A. Chowdhury, S. Kumari, A. A. Khan and S. Hussain, Selective removal of anionic dyes with exceptionally high adsorption capacity and removal of dichromate ($Cr_2O_7^{2-}$) anion using Ni-Co-S/CTAB nanocomposites and its adsorption mechanism, *J. Hazard. Mater.*, 2020, **385**, 121602, DOI: 10.1016/j.jhazmat.2019.121602.

51 S. I. Siddiqui, O. Manzoor, M. Mohsin and S. A. Chaudhry, Nigella sativa seed based nanocomposite-MnO_2/BC: An antibacterial material for photocatalytic degradation, and adsorptive removal of Methylene blue from water, *Environ. Res.*, 2019, **171**, 328–340, DOI: 10.1016/j.envres.2018.11.044.

52 P. Saha, S. Chowdhury, S. Gupta and I. Kumar, Insight into adsorption equilibrium, kinetics and thermodynamics of Malachite green onto clayey soil of Indian origin, *Chem. Eng. J.*, 2010, **165**(3), 874–882, DOI: 10.1016/j.cej.2010.10.048.

53 A. Choudhry, A. Sharma, T. A. Khan and S. A. Chaudhry, Flax seeds based magnetic hybrid nanocomposite: An advance and sustainable material for water cleansing, *J. Water Process Eng.*, 2021, **42**, 102150, DOI: 10.1016/j.jwpe.2021.102150.

54 S. L. Mera and J. D. Davies, Differential Congo red staining: the effects of pH, non-aqueous solvents and the substrate, *Histochem. J.*, 1984, **16**, 195–210, DOI: 10.1007/BF01003549.

55 S. I. Siddiqui, F. Zohra and S. A. Chaudhry, Nigella sativa seed based nanohybrid composite-Fe_2O_3-SnO_2/BC: A novel material for enhanced adsorptive removal of methylene blue from water, *Environ. Res.*, 2019, **178**, 108667, DOI: 10.1016/j.envres.2019.108667.

56 S. Neupane, S. T. Ramesh, R. Gandhimathi and P. V. Nidheesh, Pineapple leaf (Ananas comosus) powder as a biosorbent for the removal of crystal violet from aqueous solution, *Desalin. Water Treat.*, 2015, **54**(7), 2041–2054, DOI: 10.1080/19443994.2014.903867.

57 T. Etemadinia, B. Barikbin and A. Allahresani, Removal of Congo red dye from aqueous solutions using $ZnFe_2O_4$/SiO_2/Tragacanth gum magnetic nanocomposite as a novel adsorbent, *Surf. Interfaces*, 2019, **14**, 117–126, DOI: 10.1016/j.surfin.2018.10.010.

58 L. Wang and A. Wang, Adsorption characteristics of Congo red onto the chitosan/montmorillonite nanocomposite, *J. Hazard. Mater.*, 2007, **147**(3), 979–985, DOI: 10.1016/j.jhazmat.2007.01.145.

59 N. Nasseh, F. S. Arghavan, S. Rodriguez-Couto and A. Hossein Panahi, Synthesis of $FeNi_3$/SiO_2/CuS magnetic nano-composite as a novel adsorbent for Congo red dye removal, *Int. J. Environ. Anal. Chem.*, 2022, **102**(10), 2342–2362, DOI: 10.1080/03067319.2020.1754810.

60 Y. Yao, S. Miao, S. Liu, L. P. Ma, H. Sun and S. Wang, Synthesis, characterization, and adsorption properties of magnetic Fe_3O_4@graphene nanocomposite, *Chem. Eng. J.*, 2012, **184**, 326–332, DOI: 10.1016/j.cej.2011.12.017.

61 R. Jiang, J. Yao, H. Zhu, Y. Fu, Y. Guan, L. Xiao and G. Zeng, Effective decolorization of congo red in aqueous solution by adsorption and photocatalysis using novel magnetic alginate/γ-Fe_2O_3/CdS nanocomposite, *Desalin. Water Treat.*, 2014, **52**(1–3), 238–247, DOI: 10.1080/19443994.2013.787551.

62 J. Jumadi, A. Kamari, N. A. Rahim, S. T. S. Wong, S. N. M. Yusoff, S. Ishak and S. Kumaran, Removal of Methylene blue and Congo red by magnetic chitosan nanocomposite: Characterization and adsorption studies, *Journal of Physics: Conference Series*, IOP Publishing, 2019, vol. 1397, no. 1, p. 012027. , DOI: 10.1088/1742-6596/1397/1/012027.

63 S. Razzaq, M. Akhtar, S. Zulfiqar, S. Zafar, I. Shakir, P. O. Agboola and M. F. Warsi, Adsorption removal of Congo red onto L-cysteine/rGO/PANI nanocomposite: equilibrium, kinetics and thermodynamic studies, *J. Taibah Univ. Sci.*, 2021, **15**(1), 50–62, DOI: 10.1080/16583655.2021.1876351.

64 H. Y. Zhu, Y. Q. Fu, R. Jiang, J. H. Jiang, L. Xiao, G. M. Zeng and Y. Wang, Adsorption removal of Congo red onto magnetic cellulose/Fe_3O_4/activated carbon composite: Equilibrium, kinetic and thermodynamic studies, *Chem. Eng. J.*, 2011, **173**(2), 494–502, DOI: 10.1016/j.cej.2011.08.020.

65 E. A. Dil, M. Ghaedi, A. Asfaram and A. A. Bazrafshan, Ultrasound wave assisted adsorption of Congo red using gold-magnetic nanocomposite loaded on activated carbon: Optimization of process parameters, *Ultrason. Sonochem.*, 2018, **46**, 99–105, DOI: 10.1016/j.ultsonch.2018.02.040.

66 L. Wang and A. Wang, Adsorption behaviors of Congo red on the N, O-carboxymethyl-chitosan/montmorillonite nanocomposite, *Chem. Eng. J.*, 2008, **143**(1–3), 43–50, DOI: 10.1016/j.cej.2007.12.007.

67 G. Yang, Q. Huang, H. Huang, J. Chen, Y. Lei, F. Deng and Y. Wei, Preparation of cationic poly (ionic liquids) functionalization of silica nanoparticles via multicomponent condensation reaction with significant enhancement of adsorption capacity, *J. Mol. Liq.*, 2020, **300**, 112267, DOI: 10.1016/j.molliq.2019.112267.

68 R. Foroutan, R. Mohammadi and B. Ramavandi, Elimination performance of Methylene blue, Methyl violet, and Nile blue from aqueous media using AC/$CoFe_2O_4$ as a recyclable magnetic composite, *Environ. Sci. Pollut. Res.*, 2019, **26**, 19523–19539, DOI: 10.1007/s11356-019-05282-z.

69 B. Kavitha and R. Karthiga, Synthesis and characterization of $CuWO_4$ as nano-adsorbent for removal of Nile blue and its antimicrobial studies., *J. Mater. Environ. Sci.*, 2020, **11**(1), 57–68.

70 S. Abbasi and H. Noorizadeh, Adsorption of Nile blue A from aqueous solution by different nanostructured carbon adsorbents, *Carbon Lett.*, 2017, **23**, 30–37, DOI: 10.5714/CL.2017.23.030.

71 S. Aly, A. M. El-Sayed, K. M. Tharwat, M. A. Mahmoud, A. M. Khaled, A. M. Gad and A. T. Mahmoud, Adsorption of Nile blue dye using guava leaf powder, *Int. J. Eng. Res.*, 2019, **8**(12), 69–72.

72 H. Man, Y. Nie, S. Shao, Y. Wang, Z. Wang and Y. Jiang, Fabrication of Fe_3O_4@poly(methylmethacrylate-co-glycidylmethacrylate) microspheres *via* miniemulsion polymerization using porous microspheres as templates for removal of cationic dyes, *New J. Chem.*, 2022, **46**(28), 13442–13453, DOI: 10.1039/D2NJ01440H.

73 A. F. Alali, S. F. Almojil, A. I. Almohana, A. E. Anqi, A. A. Rajhi, S. Alamri and H. A. Dhahad, Hydroxyapatite@Mn–Fe composite as a reusable sorbent for removal of Nile blue dye and Cr(VI) from polluted water, *Environ. Sci. Pollut. Res.*, 2023, **30**(7), 18419–18437, DOI: 10.1007/s11356-022-22821-3.

74 R. Foroutan, S. J. Peighambardoust, Z. Esvandi, H. Khatooni and B. Ramavandi, Evaluation of two cationic dyes removal from aqueous environments using CNT/MgO/$CuFe_2O_4$ magnetic composite powder: A comparative study, *J. Environ. Chem. Eng.*, 2021, **9**(2), 104752, DOI: 10.1016/j.jece.2020.104752.

75 I. Safarik, P. Lunackova, E. Mosiniewicz-Szablewska, F. Weyda and M. Safarikova, Adsorption of water-soluble organic dyes on ferrofluid-modified sawdust, *Holzforschung*, 2007, **61**(3), 247–253, DOI: 10.1515/HF.2007.060.

76 Z. Esvandi, R. Foroutan, S. J. Peighambardoust, A. Akbari and B. Ramavandi, Uptake of anionic and cationic dyes from water using natural clay and clay/starch/$MnFe_2O_4$ magnetic nanocomposite, *Surf. Interfaces*, 2020, **21**, 100754, DOI: 10.1016/j.surfin.2020.100754.

77 A. M. Rajabi and S. B. Ardakani, Effects of natural-zeolite additive on mechanical and physicochemical properties of clayey soils, *J. Mater. Civ. Eng.*, 2020, **32**(10), 04020306.

78 D. Akbarimehr, A. Eslami, E. Aflaki and R. Imam, Using empirical correlations and artificial neural network to estimate compressibility of low plasticity clays, *Arabian J. Geosci.*, 2020, **13**(22), 1–11.

79 D. Akbarimehr and S. M. M. M. Hosseini, Elasto-plastic characteristics of the clay soil mixed with rubber waste using cyclic triaxial test results, *Arabian J. Geosci.*, 2022, **15**, 1280.